GEOPHYSICS, VOL. 74, NO. 6 (NOVEMBER-DECEMBER 2009); P. WCD15–WCD27, 15 FIGS.
10.1190/1.3251271

Direct nonlinear inversion of multiparameter 1D elastic media using the inverse scattering series

Haiyan Zhang[1] and Arthur B. Weglein[2]

ABSTRACT

In the direct nonlinear inversion method and in algorithms for 1D elastic media, P-wave velocity, S-wave velocity, and density are depth dependent. "Direct nonlinear" means that the method uses explicit formulas that (1) input data and directly output changes in material properties without the need for indirect procedures such as model matching, searching, optimization, or other assumed aligned objectives or proxies and that (2) the algorithms recognize and directly invert the intrinsic nonlinear relationship between changes in material properties and the recorded reflection wavefields. To achieve full elastic inversion, all components of data (such as PP, SP, and SS data) are needed. The method assumes that only data and reference medium properties are input, and terms in the inverse series for moving mislocated reflectors resulting from the linear inverse term are separated from amplitude correction terms. Although in principle this direct inversion approach requires all components of elastic data, synthetic tests indicate that a consistent value-added result may be achieved given only PP data measurements, as long as the PP data are used to approximately synthesize the PS and SP components. Further value would be derived from measuring all components of the data as the method requires. If all components of data are available, one consistent method can solve for all of the second terms (the first terms beyond linear). The explicit nonlinear inversion formulas provide an unambiguous data requirement message as well as conceptual and practical added value beyond both linear approaches and all indirect methods.

INTRODUCTION

The objective of seismic data processing is to use measured reflection data to determine the spatial locations or images of reflectors and the changes in mechanical properties across the imaged reflectors. There are many methods for achieving those two interrelated goals, and all of them can be effective when their assumptions are satisfied.

The standard methods used today in exploration seismology assume knowledge of properties of the subsurface medium above the reflector of interest. They also assume that a forward relationship relates the angle-dependent PP reflection data to changes in properties across the reflector. That relationship can be solved by linear forward approximation (PP Bortfeld approximation) or by model matching, full waveform inversion, iterative linear updating, or global searching using the nonlinear forward PP Zoeppritz relationship (Sheriff and Geldart, 1994). Because P-waves nonnormally incident on an elastic interface can produce S-waves, and vice versa (converted waves; Aki and Richards, 2002), the elastic data generally contain four components: PP, PS, SP, and SS.

In this paper, we provide a new understanding and firmer foundation for addressing the problem of finding the changes in physical properties across a reflector as well as understanding the fundamental new algorithms that emerge from that framework. We begin by defining the difference between direct and indirect algorithms. The current methods (listed in the previous paragraph) for estimating properties of target reflectors are indirect. Indirect inversion methods seek an aligned objective, cost function, or proxy in place of a direct inverse solution. Indirect inverse methods start with a forward problem and, one way or another, seek to solve the forward problem in an inverse sense for changes in mechanical properties in terms of input reflection data. Hence, the foundation of all current target identification methods is the forward or modeling problem, and the concomitant indirect inversion methods are based on model matching.

In contrast, the foundation of the method described here is a direct inverse solution. That distinction and its implications, meaning, and consequences are the central point here. The direct inverse target identification method recognizes the innate nonlinear relationship between the change in any (and every) mechanical property that

Manuscript received by the Editor 31 December 2008; revised manuscript received 9 July 2009; published online 15 December 2009.
[1]Formerly University of Houston, Department of Physics, Houston, Texas, U.S.A.; presently ConocoPhillips, Houston, Texas. E-mail: haiyan.zhang@conocophillips.com.
[2]University of Houston, Houston, Texas, U.S.A. E-mail: aweglein@uh.edu.

changes at a reflector and the reflection data that emanate from that reflector. It provides direct explicit relationships for the linear and nonlinear approximation for those property changes in terms of measured reflection data. That process provides the data and algorithms required for a direct nonlinear solution.

The equation for the linear estimate is the exact equation for the linear estimate. The equation for the quadratic estimate is the exact equation for the quadratic estimate, and so on for each higher term. There is no search, no cost function, no model matching, but an order by order in the data direct solution, where each step is exact for its indicated order of approximation. The unambiguous message delivered by those exact linear and higher-order equations is that all components of PP, SP, SS, and PS data are directly called upon and needed in the direct inverse amplitude variation with offset (AVO) solution.

Communicating this conceptual and fundamental message concerning direct and indirect methods and their distinction and significant consequences is a major goal of this paper. A secondary goal is to provide an approach to navigate the need for multicomponent data when one has only towed-streamer PP measurements and the other components are synthesized from the PP data. That synthesis falls short of real measurements but is better than placing zeros where the multicomponent data are called for.

This need for multicomponent data for the direct elimination of free-surface and internal multiples in ocean-bottom and onshore applications was recognized in early work (Matson, 1997). These applications required a homogeneous elastic reference medium that agreed with ocean-bottom or near-surface onshore properties. The specific AVO problem that we address here has a known elastic half-space (as the reference medium) over an unknown elastic half-space, the simplest realistic model for amplitude analysis. We provide the direct inverse solution to that simplest realistic 1D AVO model. Hence, although it might seem to be a simple model, it has in fact had a direct solution, and this direct inversion procedure differs from all current AVO methods.

Our method derives from the only direct inverse method for multidimensional acoustic, elastic, and anelastic media — the inverse scattering series. The inverse scattering series is direct and it allows all processing goals to be achieved directly in terms of only the data.

The question we ask is whether the inverse scattering series, with all its potential and already-delivered dividend for removing free-surface and internal multiples, can be pointed at the simplest AVO problem that has no previous direct solution. Toward that end and focused goal, we assume that all multiples have been removed, the overburden is known, and the depth of the single horizontal reflector is given. Then we can ask for a direct inverse solution for the changes in elastic properties across that one reflector. To get to that algorithm, we formulate the direct elastic inverse scattering series in a 1D earth and then isolate the direct AVO task by identifying and ignoring tasks that are assumed to have been achieved, i.e., free-surface and internal multiple removal and depth imaging of the location of the reflector.

Hence, the formidable and new mathematics that deal with everything that an elastic direct inversion method requires are developed before identifying the part of the elastic inverse series that deals only with direct AVO analysis. It is daunting to separate and isolate the AVO-only terms from the tangle of other terms. However, there appears to be no other way to reach the direct nonlinear AVO-isolated terms without starting with the overarching complete direct elastic inverse scattering series.

THE INVERSE SCATTERING SERIES AND ISOLATED TASK SUBSERIES

What makes the inverse scattering series powerful is the task-isolated subseries, which is a subset of the entire series that acts as though only one task is performed for that subset (Weglein et al., 2003). All of these subseries act in a certain processing sequence so that the total seismic data can be processed accordingly: (1) free-surface multiple removal, (2) internal multiple removal, (3) depth imaging without velocity, and (4) inversion or target identification. Because the entire process requires only reflection data and reference medium information, it is reasonable to assume that these intermediate steps (i.e., all of the derived subseries associated with achieving that objective) would be attainable with only the reference medium and reflection data — no subsurface medium information is required.

The free-surface multiple removal and internal multiple attenuation subseries are presented by Carvalho (1992), Araújo (1994), Weglein et al. (1997), and Matson (1997). Those two multiple procedures are independent of model type, i.e., they work for acoustic, elastic, and anelastic media. Studies on taking internal multiples from attenuation to elimination are under way (Ramírez and Weglein, 2005). The task-specific subseries associated with primary reflections (i.e., for imaging and inversion) also have been progressed. One subseries is imaging without velocity for one parameter in 1D and then 2D acoustic media (Weglein et al., 2002; Liu and Weglein, 2003; Shaw and Weglein, 2003, 2004; Shaw et al., 2003a, 2003b, 2004; Liu et al., 2004; Liu et al., 2005). A second subseries is direct nonlinear inversion for multiparameter 1D acoustic and then elastic media (Zhang and Weglein, 2005). Recent work (Innanen and Weglein, 2004, 2005) suggests that some well-known seismic processing tasks associated with resolution enhancement (i.e., Q-compensation) can be accomplished within the task-separated inverse scattering series framework. In this paper, we focus on direct nonlinear inversion.

Specifically, the stages within the strategy for primary reflections are as follows:

1) 1D earth with one parameter, velocity as a function of depth, a normal incidence wave
2) 1D earth with one parameter varying (velocity as a function of depth) offset data, one shot record
3) 2D earth with one parameter varying (velocity varying in x and z), a suite of shot records
4) 1D acoustic earth with two parameters varying (velocity and density), one propagation velocity, one shot record of PP data
5) 1D elastic earth, two elastic isotropic parameters and density varying, two wavespeeds for P- and S-waves, shot records collected for PP, PS, SP, and SS waves

Here, we add another step of direct nonlinear inversion and isolate tasks specifically associated with primary reflectors to the 1D elastic earth case (stage 5). Our model is elastic; a study with an acoustic model is presented by Zhang and Weglein (2005). We take these steps and learn to navigate through this complexity, steering it toward useful and powerful algorithms.

However, more realism adds more complexity with more inverse issues to be addressed. Following the task-separation strategy, we ask ourselves, what kind of tasks should we expect in this more complex, elastic setting? For the acoustic case, for example, the acoustic medium supports only P-waves, so only one reference velocity (P-

wave velocity) is involved. Therefore, when only one velocity is incorrect (i.e., poorly estimated), there is only one mislocation for each parameter and the imaging terms need to correct only this one mislocation. When we extend our previous work on the two-parameter acoustic case to the three-parameter elastic case, there will be four mislocations because there are two reference velocities (P- and S-wave velocities). Our reasoning is that the elastic medium supports P- and S-wave propagation, so both P- and S-wave velocities are involved. When these velocities are incorrect, there are generally four mislocations, one for each of the four possible combinations of the two wrong velocities.

In this paper, we present a nonlinear inversion term for a three-parameter 1D elastic medium. We demonstrate that under the inverse scattering series inversion framework, all components of the data are needed to perform full elastic inversion. Where we do not have all component data (i.e., only PP data are available), we obtain encouraging inversion results by constructing other components of data from the PP data. This means we could perform elastic inversion by using only pressure measurements (i.e., towed-streamer data). Where all components of data are available, we provide a consistent method to solve for second-order terms.

BACKGROUND FOR 2D ELASTIC INVERSION

In this section, we consider the inversion problem in two dimensions for an elastic medium. We start with the displacement space; then, for convenience (see, e.g., Aki and Richards, 2002), we change the basis and transform the equations to PS space. Here, the way to denote displacement space and PS space depends mainly on the basis function chosen in each space. In displacement space, we chose the displacement field $\mathbf{u}$ as the basis function. In PS space, we chose $\mathbf{\Phi}$ as the basis function. The differential operator that describes the wave propagation in the reference medium (L_0, defined below) would be diagonal in PS space, and P- and S-wave-related operators would be separated in each of the two nonzero elements. Finally, we demonstrate the elastic inversion in the PS domain.

Displacement space

We begin with some basic equations in the displacement space (Matson, 1997):

$$L\mathbf{u} = \mathbf{f}, \tag{1}$$

$$L_0\mathbf{u} = \mathbf{f}, \tag{2}$$

$$LG = \delta, \tag{3}$$

$$L_0G_0 = \delta, \tag{4}$$

where L and L_0 are the differential operators that describe the wave propagation in the actual and reference medium, respectively; $\mathbf{u}$ and $\mathbf{f}$ are the corresponding displacement and source terms; and G and G_0 are the corresponding Green's operators for the actual and reference medium. In the following, the quantities with a zero subscript relate to the reference medium; those without a subscript relate to the actual medium.

Closely following Weglein et al. (1997), Weglein et al. (2002), and Weglein et al. (2003), defining the perturbation $V = L_0 - L$, we find the Lippmann-Schwinger equation for the elastic media in the displacement space:

$$G = G_0 + G_0VG. \tag{5}$$

Iterating this equation back into itself generates the Born series:

$$G = G_0 + G_0VG_0 + G_0VG_0VG_0 + \cdots. \tag{6}$$

We define the data D as the measured values of the scattered wavefield $G - G_0$. Then, on the measurement surface, we have

$$D = G_0VG_0 + G_0VG_0VG_0 + \cdots. \tag{7}$$

Expanding V as a series in orders of D, we have

$$V = V_1 + V_2 + V_3 + \cdots. \tag{8}$$

Here, the subscript i in V_i ($i = 1,2,3,\ldots$) denotes the ith-order portion of V in the data. Substituting equation 8 into equation 7, evaluating equation 7, and setting terms of equal order in the data equal, the following equations that determine $V_1, V_2, \ldots$ from D and G_0 are obtained:

$$D = G_0V_1G_0, \tag{9}$$

$$0 = G_0V_2G_0 + G_0V_1G_0V_1G_0, \ldots. \tag{10}$$

In the actual medium, the 2D elastic wave equation is (A. B. Weglein and R. H. Stolt, personal communication, 1992)

$$\begin{aligned} L\mathbf{u} \equiv & \left[\rho\omega^2\begin{pmatrix}1 & 0\\ 0 & 1\end{pmatrix}\right. \\ & \left. + \begin{pmatrix}\partial_1\gamma\partial_1 + \partial_2\mu\partial_2 & \partial_1(\gamma - 2\mu)\partial_2 + \partial_2\mu\partial_1\\ \partial_2(\gamma - 2\mu)\partial_1 + \partial_1\mu\partial_2 & \partial_2\gamma\partial_2 + \partial_1\mu\partial_1\end{pmatrix}\right]\begin{bmatrix}u_1\\ u_2\end{bmatrix} \\ = & \mathbf{f}, \end{aligned} \tag{11}$$

where $\mathbf{u} = \begin{bmatrix}u_1\\ u_2\end{bmatrix}$ = displacement; ρ is density; γ is P-wave modulus $\equiv\rho\alpha^2$, where α = P-wave velocity; μ = shear modulus $\equiv\rho\beta^2$, where β = S-wave velocity; ω = temporal frequency (angular); ∂_1 and ∂_2 denote the derivative over x and z, respectively; and $\mathbf{f}$ is the source term.

For constant $(\rho,\gamma,\mu) = (\rho_0,\gamma_0,\mu_0)$, $(\alpha,\beta) = (\alpha_0,\beta_0)$, the operator L becomes

$$L_0 \equiv \left[\rho_0\omega^2\begin{pmatrix}1 & 0\\ 0 & 1\end{pmatrix} + \begin{pmatrix}\gamma_0\partial_1^2 + \mu_0\partial_2^2 & (\gamma_0 - \mu_0)\partial_1\partial_2\\ (\gamma_0 - \mu_0)\partial_1\partial_2 & \mu_0\partial_1^2 + \gamma_0\partial_2^2\end{pmatrix}\right]. \tag{12}$$

Then,

$$\begin{aligned} V \equiv & L_0 - L \\ = & -\rho_0\begin{bmatrix} a_\rho\omega^2 + \alpha_0^2\partial_1a_\gamma\partial_1 + \beta_0^2\partial_2a_\mu\partial_2 & \partial_1(\alpha_0^2a_\gamma - 2\beta_0^2a_\mu)\partial_2 + \beta_0^2\partial_2a_\mu\partial_1\\ \partial_2(\alpha_0^2a_\gamma - 2\beta_0^2a_\mu)\partial_1 + \beta_0^2\partial_1a_\mu\partial_2 & a_\rho\omega^2 + \alpha_0^2\partial_2a_\gamma\partial_2 + \beta_0^2\partial_1a_\mu\partial_1\end{bmatrix}, \end{aligned} \tag{13}$$

where $a_\rho \equiv (\rho/\rho_0) - 1$, $a_\gamma \equiv (\gamma/\gamma_0) - 1$, and $a_\mu \equiv (\mu/\mu_0) - 1$ are the three parameters we choose for the elastic inversion. Similar to equation 8, a_ρ, a_γ, and a_μ can be expanded as

$$a_\rho = a_\rho^{(1)} + a_\rho^{(2)} + a_\rho^{(3)} + \cdots, \tag{14}$$

$$a_\gamma = a_\gamma^{(1)} + a_\gamma^{(2)} + a_\gamma^{(3)} + \cdots, \tag{15}$$

$$a_\mu = a_\mu^{(1)} + a_\mu^{(2)} + a_\mu^{(3)} + \cdots, \tag{16}$$

where the superscripts (1), (2), and (3) denote the linear, first nonlinear or second term, and the third term, respectively.

For a 1D earth (i.e., where a_ρ, a_γ, and a_μ are functions only of depth z), equation 13 becomes

$$V=-\rho_0\begin{bmatrix} a_\rho\omega^2+\alpha_0^2a_\gamma\partial_1^2+\beta_0^2\partial_2a_\mu\partial_2 & (\alpha_0^2a_\gamma-2\beta_0^2a_\mu)\partial_1\partial_2+\beta_0^2\partial_2a_\mu\partial_1 \\ \partial_2(\alpha_0^2a_\gamma-2\beta_0^2a_\mu)\partial_1+\beta_0^2a_\mu\partial_1\partial_2 & a_\rho\omega^2+\alpha_0^2\partial_2a_\gamma\partial_2+\beta_0^2a_\mu\partial_1^2 \end{bmatrix}. \tag{17}$$

Transforming to PS space

For convenience, we can change the basis from $\mathbf{u}=\begin{bmatrix} u_1 \\ u_2 \end{bmatrix}$ to $\begin{pmatrix} \phi^P \\ \phi^S \end{pmatrix}$ to allow L_0 to be diagonal:

$$\mathbf{\Phi}=\begin{pmatrix} \phi^{\mathrm{P}} \\ \phi^{\mathrm{S}} \end{pmatrix}=\begin{bmatrix} \gamma_0(\partial_1u_1+\partial_2u_2) \\ \mu_0(\partial_1u_2-\partial_2u_1) \end{bmatrix}. \tag{18}$$

This can be written as

$$\begin{pmatrix} \phi^{\mathrm{P}} \\ \phi^{\mathrm{S}} \end{pmatrix}=\Gamma_0\Pi\mathbf{u}, \tag{19}$$

where

$$\Pi=\begin{pmatrix} \partial_1 & \partial_2 \\ -\partial_2 & \partial_1 \end{pmatrix} \quad \text{and} \quad \Gamma_0=\begin{pmatrix} \gamma_0 & 0 \\ 0 & \mu_0 \end{pmatrix}.$$

In the reference medium, the operator L_0 will be diagonal in the new basis via a transformation

$$\hat{L}_0\equiv\Pi L_0\Pi^{-1}\Gamma_0^{-1}=\begin{pmatrix} \hat{L}_0^{\mathrm{P}} & 0 \\ 0 & \hat{L}_0^{\mathrm{S}} \end{pmatrix}, \tag{20}$$

where $\hat{L}_0$ is L_0 transformed to PS space, $\Pi^{-1}=\begin{pmatrix} \partial_1 & -\partial_2 \\ \partial_2 & \partial_1 \end{pmatrix}\nabla^{-2}$ is the inverse matrix of Π, $\hat{L}_0^{\mathrm{P}}=\omega^2/\alpha_0^2+\nabla^2$, $\hat{L}_0^{\mathrm{S}}=\omega^2/\beta_0^2+\nabla^2$, and

$$\mathbf{F}=\Pi\mathbf{f}=\begin{pmatrix} F^{\mathrm{P}} \\ F^{\mathrm{S}} \end{pmatrix}. \tag{21}$$

Then, in the PS domain, equation 2 becomes

$$\begin{pmatrix} \hat{L}_0^{\mathrm{P}} & 0 \\ 0 & \hat{L}_0^{\mathrm{S}} \end{pmatrix}\begin{pmatrix} \phi^{\mathrm{P}} \\ \phi^{\mathrm{S}} \end{pmatrix}=\begin{pmatrix} F^{\mathrm{P}} \\ F^{\mathrm{S}} \end{pmatrix}. \tag{22}$$

Because $G_0\equiv L_0^{-1}$, let $\hat{G}_0^{\mathrm{P}}=(\hat{L}_0^{\mathrm{P}})^{-1}$ and $\hat{G}_0^{\mathrm{S}}=(\hat{L}_0^{\mathrm{S}})^{-1}$. Then the displacement G_0 in the PS domain becomes

$$\hat{G}_0=\Gamma_0\Pi G_0\Pi^{-1}=\begin{pmatrix} \hat{G}_0^{\mathrm{P}} & 0 \\ 0 & \hat{G}_0^{\mathrm{S}} \end{pmatrix}. \tag{23}$$

So, in the reference medium, after transforming from the displacement domain to the PS domain, L_0 and G_0 become diagonal and there are only direct P- and S-waves, which are separated in this case.

Multiplying equation 5 from the left by the operator $\Gamma_0\Pi$ and from the right by the operator Π^{-1}, and using equation 23,

$$\begin{aligned}\Gamma_0\Pi G\Pi^{-1}&=\hat{G}_0+\hat{G}_0(\Pi V\Pi^{-1}\Gamma_0^{-1})\Gamma_0\Pi G\Pi^{-1}\\&=\hat{G}_0+\hat{G}_0\hat{V}\hat{G},\end{aligned} \tag{24}$$

where the displacement Green's operator G is transformed to the PS domain as

$$\hat{G}=\Gamma_0\Pi G\Pi^{-1}=\begin{pmatrix} \hat{G}^{\mathrm{PP}} & \hat{G}^{\mathrm{PS}} \\ \hat{G}^{\mathrm{SP}} & \hat{G}^{\mathrm{SS}} \end{pmatrix}. \tag{25}$$

The perturbation V in the PS domain becomes

$$\hat{V}=\Pi V\Pi^{-1}\Gamma_0^{-1}=\begin{pmatrix} \hat{V}^{\mathrm{PP}} & \hat{V}^{\mathrm{PS}} \\ \hat{V}^{\mathrm{SP}} & \hat{V}^{\mathrm{SS}} \end{pmatrix}, \tag{26}$$

where the left superscripts of the matrix elements represent the type of measurement and the right ones are the source type.

Similarly, applying the PS transformation to the entire inverse series gives

$$\hat{V}=\hat{V}_1+\hat{V}_2+\hat{V}_3+\cdots. \tag{27}$$

It follows from equations 24 and 27 that

$$\hat{D}=\hat{G}_0\hat{V}_1\hat{G}_0, \tag{28}$$

$$\hat{G}_0\hat{V}_2\hat{G}_0=-\hat{G}_0\hat{V}_1\hat{G}_0\hat{V}_1\hat{G}_0,\ldots, \tag{29}$$

where

$$\hat{D}=\begin{pmatrix} \hat{D}^{\mathrm{PP}} & \hat{D}^{\mathrm{PS}} \\ \hat{D}^{\mathrm{SP}} & \hat{D}^{\mathrm{SS}} \end{pmatrix}$$

are the data in the PS domain.

LINEAR INVERSION OF A 1D ELASTIC MEDIUM

We now look at the linear terms in the inverse series. Writing equation 28 in matrix form,

$$\begin{pmatrix} \hat{D}^{\mathrm{PP}} & \hat{D}^{\mathrm{PS}} \\ \hat{D}^{\mathrm{SP}} & \hat{D}^{\mathrm{SS}} \end{pmatrix}=\begin{pmatrix} \hat{G}_0^{\mathrm{P}} & 0 \\ 0 & \hat{G}_0^{\mathrm{S}} \end{pmatrix}\begin{pmatrix} \hat{V}_1^{\mathrm{PP}} & \hat{V}_1^{\mathrm{PS}} \\ \hat{V}_1^{\mathrm{SP}} & \hat{V}_1^{\mathrm{SS}} \end{pmatrix}\begin{pmatrix} \hat{G}_0^{\mathrm{P}} & 0 \\ 0 & \hat{G}_0^{\mathrm{S}} \end{pmatrix}, \tag{30}$$

leads to four equations:

$$\hat{D}^{\mathrm{PP}}=\hat{G}_0^{\mathrm{P}}\hat{V}_1^{\mathrm{PP}}\hat{G}_0^{\mathrm{P}}, \tag{31}$$

$$\hat{D}^{\mathrm{PS}}=\hat{G}_0^{\mathrm{P}}\hat{V}_1^{\mathrm{PS}}\hat{G}_0^{\mathrm{S}}, \tag{32}$$

$$\hat{D}^{\mathrm{SP}}=\hat{G}_0^{\mathrm{S}}\hat{V}_1^{\mathrm{SP}}\hat{G}_0^{\mathrm{P}}, \tag{33}$$

$$\hat{D}^{SS} = \hat{G}_0^S \hat{V}_1^{SS} \hat{G}_0^S. \tag{34}$$

For $z_s = z_g = 0$, Fourier transforming equations 31–34 from the $(x_s,z_s;x_g,z_g;\omega)$ domain to the $(k_s,z_s;k_g,z_g;\omega)$ domain, we get the following four equations relating the linear components of the three elastic parameters and the four data types (Zhang, 2006):

$$\begin{aligned}\tilde{D}^{PP}(k_g,0;-k_g,0;\omega) &= -\frac{1}{4}\left(1-\frac{k_g^2}{\nu_g^2}\right)\tilde{a}_\rho^{(1)}(-2\nu_g) - \frac{1}{4}\left(1+\frac{k_g^2}{\nu_g^2}\right)\\ &\times\tilde{a}_\gamma^{(1)}(-2\nu_g) + \frac{2k_g^2\beta_0^2}{(\nu_g^2+k_g^2)\alpha_0^2}\tilde{a}_\mu^{(1)}(-2\nu_g),\end{aligned} \tag{35}$$

$$\begin{aligned}\tilde{D}^{PS}(\nu_g,\eta_g) &= -\frac{1}{4}\left(\frac{k_g}{\nu_g}+\frac{k_g}{\eta_g}\right)\tilde{a}_\rho^{(1)}(-\nu_g-\eta_g) - \frac{\beta_0^2}{2\omega^2}k_g(\nu_g+\eta_g)\\ &\times\left(1-\frac{k_g^2}{\nu_g\eta_g}\right)\tilde{a}_\mu^{(1)}(-\nu_g-\eta_g),\end{aligned} \tag{36}$$

$$\begin{aligned}\tilde{D}^{SP}(\nu_g,\eta_g) &= \frac{1}{4}\left(\frac{k_g}{\nu_g}+\frac{k_g}{\eta_g}\right)\tilde{a}_\rho^{(1)}(-\nu_g-\eta_g) + \frac{\beta_0^2}{2\omega^2}k_g(\nu_g+\eta_g)\\ &\times\left(1-\frac{k_g^2}{\nu_g\eta_g}\right)\tilde{a}_\mu^{(1)}(-\nu_g-\eta_g),\end{aligned} \tag{37}$$

$$\begin{aligned}\tilde{D}^{SS}(k_g,\eta_g) &= -\frac{1}{4}\left(1-\frac{k_g^2}{\eta_g^2}\right)\tilde{a}_\rho^{(1)}(-2\eta_g)\\ &-\left[\frac{\eta_g^2+k_g^2}{4\eta_g^2}-\frac{2k_g^2}{\eta_g^2+k_g^2}\right]\tilde{a}_\mu^{(1)}(-2\eta_g),\end{aligned} \tag{38}$$

where $\nu_g^2 + k_g^2 = (\omega^2/\alpha_0^2)$ and $\eta_g^2 + k_g^2 = (\omega^2/\beta_0^2)$.

As shown by Zhang and Weglein (2005), when the work on the two-parameter acoustic case is extended to the three-parameter elastic case, it is not just adding one more parameter — more issues are involved. Even for the linear case, the linear solutions found in equations 35–38 are much more complicated than those of the acoustic case. For instance, four sets of linear parameter estimates are produced from the four components of the data. Also, generally four distinct reflector mislocations arise from the two reference velocities (P- and S-wave velocities).

For the P-wave incidence on a 1D single interface case (see Figure 1), using $k_g^2/\nu_g^2 = \tan^2\theta$ and $k_g^2/(\nu_g^2+k_g^2) = \sin^2\theta$, where θ is the P-wave incident angle, equation 35 becomes

$$\begin{aligned}\tilde{D}^{PP}(\nu_g,\theta) &= -\frac{1}{4}(1-\tan^2\theta)\tilde{a}_\rho^{(1)}(-2\nu_g)\\ &-\frac{1}{4}(1+\tan^2\theta)\tilde{a}_\gamma^{(1)}(-2\nu_g)\\ &+\frac{2\beta_0^2\sin^2\theta}{\alpha_0^2}\tilde{a}_\mu^{(1)}(-2\nu_g).\end{aligned} \tag{39}$$

Equation 39 is used for the numerical test in the next section. It seems straightforward to use the data at three angles to obtain the linear inversion of a_ρ, a_γ, and a_μ, and this is what we do. However, this requires a whole new understanding of the definition of the data, a point discussed by Weglein (2007).

DIRECT NONLINEAR INVERSION OF A 1D ELASTIC MEDIUM

We next look at the second-order terms in the inverse series. Writing equation 29 in matrix form,

$$\begin{aligned}\begin{pmatrix}\hat{G}_0^P & 0\\ 0 & \hat{G}_0^S\end{pmatrix}\begin{pmatrix}\hat{V}_2^{PP} & \hat{V}_2^{PS}\\ \hat{V}_2^{SP} & \hat{V}_2^{SS}\end{pmatrix}\begin{pmatrix}\hat{G}_0^P & 0\\ 0 & \hat{G}_0^S\end{pmatrix} &= -\begin{pmatrix}\hat{G}_0^P & 0\\ 0 & \hat{G}_0^S\end{pmatrix}\\ &\times\begin{pmatrix}\hat{V}_1^{PP} & \hat{V}_1^{PS}\\ \hat{V}_1^{SP} & \hat{V}_1^{SS}\end{pmatrix}\begin{pmatrix}\hat{G}_0^P & 0\\ 0 & \hat{G}_0^S\end{pmatrix}\begin{pmatrix}\hat{V}_1^{PP} & \hat{V}_1^{PS}\\ \hat{V}_1^{SP} & \hat{V}_1^{SS}\end{pmatrix}\begin{pmatrix}\hat{G}_0^P & 0\\ 0 & \hat{G}_0^S\end{pmatrix},\end{aligned} \tag{40}$$

leads to four equations:

$$\hat{G}_0^P\hat{V}_2^{PP}\hat{G}_0^P = -\hat{G}_0^P\hat{V}_1^{PP}\hat{G}_0^P\hat{V}_1^{PP}\hat{G}_0^P - \hat{G}_0^P\hat{V}_1^{PS}\hat{G}_0^S\hat{V}_1^{SP}\hat{G}_0^P, \tag{41}$$

$$\hat{G}_0^P\hat{V}_2^{PS}\hat{G}_0^S = -\hat{G}_0^P\hat{V}_1^{PP}\hat{G}_0^P\hat{V}_1^{PS}\hat{G}_0^S - \hat{G}_0^P\hat{V}_1^{PS}\hat{G}_0^S\hat{V}_1^{SS}\hat{G}_0^S, \tag{42}$$

$$\hat{G}_0^S\hat{V}_2^{SP}\hat{G}_0^P = -\hat{G}_0^S\hat{V}_1^{SP}\hat{G}_0^P\hat{V}_1^{PP}\hat{G}_0^P - \hat{G}_0^S\hat{V}_1^{SS}\hat{G}_0^S\hat{V}_1^{SP}\hat{G}_0^P, \tag{43}$$

$$\hat{G}_0^S\hat{V}_2^{SS}\hat{G}_0^S = -\hat{G}_0^S\hat{V}_1^{SP}\hat{G}_0^P\hat{V}_1^{PS}\hat{G}_0^S - \hat{G}_0^S\hat{V}_1^{SS}\hat{G}_0^S\hat{V}_1^{SS}\hat{G}_0^S. \tag{44}$$

Because $\hat{V}_1^{PP}$ relates to $\hat{D}^{PP}$, $\hat{V}_1^{PS}$ relates to $\hat{D}^{PS}$, and so on, all components of the data will be coupled in the nonlinear elastic inversion. We cannot perform the full direct nonlinear inversion without knowing all components of the data.

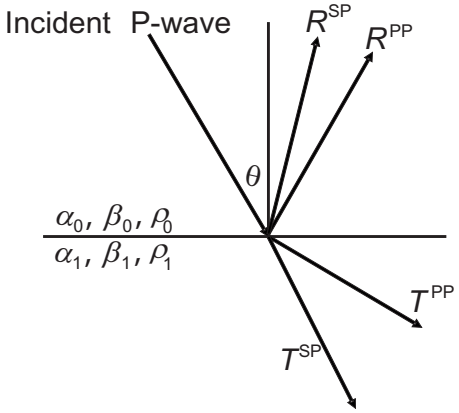

Figure 1. Response of an incident P-wave on a planar elastic interface. Parameters α_0, β_0, and ρ_0 are the P-wave velocity, S-wave velocity, and density of the upper layer, respectively; α_1, β_1, and ρ_1 denote the P-wave velocity, S-wave velocity, and density of the lower layer; and R^{PP}, R^{SP}, T^{PP}, and T^{SP} denote the coefficients of the reflected P-wave, the reflected S-wave, the transmitted P-wave, and the transmitted S-wave, respectively (Foster et al., 1997).

However, in some situations (e.g., the towed-streamer case), we do not have all components of data available. A particular nonlinear approach presented in the next section side steps part of this complexity and addresses our typical lack of all components of elastic data. In it, we use $\hat{D}^{PP}$ as the fundamental data input, perform a reduced form of nonlinear elastic inversion, and concurrently ask, What beyond-linear value does this simpler framework add? We will see from the numerical tests presented in the following section.

$\hat{D}^{PP}$ only approach

Assuming only $\hat{D}^{PP}$ are available, we first compute the linear solution for $a_\rho^{(1)}$, $a_\gamma^{(1)}$, and $a_\mu^{(1)}$ from equation 35. Then, substituting the solution into equations 36 and 37, we synthesize the other components of data, $\hat{D}^{PS}$ and $\hat{D}^{SP}$, required for equation 41. Finally, using the given $\hat{D}^{PP}$ and the synthesized data, we perform the nonlinear elastic inversion, getting the following second-order (first term beyond linear) elastic inversion solution from equation 41:

$$
\begin{aligned}
&(1-\tan^2\theta)a_\rho^{(2)}(z)+(1+\tan^2\theta)a_\gamma^{(2)}(z)-8b^2\sin^2\theta a_\mu^{(2)}(z)\\
&=-\frac{1}{2}(\tan^4\theta-1)[a_\gamma^{(1)}(z)]^2+\frac{\tan^2\theta}{\cos^2\theta}a_\gamma^{(1)}(z)a_\rho^{(1)}(z)\\
&\quad+\frac{1}{2}\left[(1-\tan^4\theta)-\frac{2}{C+1}\left(\frac{1}{C}\right)\left(\frac{\alpha_0^2}{\beta_0^2}-1\right)\frac{\tan^2\theta}{\cos^2\theta}\right]\\
&\quad\times[a_\rho^{(1)}(z)]^2-4b^2\left[\tan^2\theta-\frac{2}{C+1}\left(\frac{1}{2C}\right)\left(\frac{\alpha_0^2}{\beta_0^2}-1\right)\right.\\
&\quad\left.\times\tan^4\theta\right]a_\rho^{(1)}(z)a_\mu^{(1)}(z)+2b^4\left(\tan^2\theta-\frac{\alpha_0^2}{\beta_0^2}\right)\\
&\quad\times\left[2\sin^2\theta-\frac{2}{C+1}\frac{1}{C}\left(\frac{\alpha_0^2}{\beta_0^2}-1\right)\tan^2\theta\right]\\
&\quad\times[a_\mu^{(1)}(z)]^2-\frac{1}{2}\left(\frac{1}{\cos^4\theta}\right)a_\gamma^{(1)\prime}(z)\\
&\quad\times\int_0^z dz'[a_\gamma^{(1)}(z')-a_\rho^{(1)}(z')]\\
&\quad-\frac{1}{2}(1-\tan^4\theta)a_\rho^{(1)\prime}(z)\int_0^z dz'[a_\gamma^{(1)}(z')-a_\rho^{(1)}(z')]\\
&\quad+4b^2\tan^2\theta a_\mu^{(1)\prime}(z)\int_0^z dz'[a_\gamma^{(1)}(z')-a_\rho^{(1)}(z')]\\
&\quad+\frac{2}{C+1}\frac{1}{C}\left(\frac{\alpha_0^2}{\beta_0^2}-1\right)\tan^2\theta(\tan^2\theta-C)b^2\int_0^z dz'\\
&\quad\times a_{\mu_z}^{(1)}\left(\frac{(C-1)z'+2z}{(C+1)}\right)a_\rho^{(1)}(z')-\frac{2}{C+1}\frac{2}{C}\\
&\quad\times\left(\frac{\alpha_0^2}{\beta_0^2}-1\right)\tan^2\theta\left(\tan^2\theta-\frac{\alpha_0^2}{\beta_0^2}\right)b^4\int_0^z dz'\\
&\quad\times a_{\mu_z}^{(1)}\left(\frac{(C-1)z'+2z}{(C+1)}\right)\\
&\quad\times a_\mu^{(1)}(z')+\frac{2}{C+1}\frac{1}{C}\left(\frac{\alpha_0^2}{\beta_0^2}-1\right)\tan^2\theta(\tan^2\theta+C)\\
&\quad\times b^2\int_0^z dz'a_\mu^{(1)}(z')\\
&\quad\times a_{\rho_z}^{(1)}\left(\frac{(C-1)z'+2z}{(C+1)}\right)-\frac{2}{C+1}\frac{1}{2C}\\
&\quad\times\left(\frac{\alpha_0^2}{\beta_0^2}-1\right)\tan^2\theta(\tan^2\theta+1)\int_0^z dz'a_\rho^{(1)}(z')\\
&\quad\times a_{\rho_z}^{(1)}\left(\frac{(C-1)z'+2z}{(C+1)}\right),
\end{aligned}
\tag{45}
$$

where $a_{\rho z}^{(1)}(((C-1)z'+2z)/(C+1))=d[a_\rho^{(1)}(((C-1)z'+2z)/(C+1))]/dz$, $b=\beta_0/\alpha_0$, and $C=\eta_g/\nu_g=(\sqrt{1-b^2\sin^2\theta})/(b\sqrt{1-\sin^2\theta})$.

The first five terms on the right side of equation 45 are inversion terms; they contribute to parameter predictions. The other terms on the right side of the equation are imaging terms. These arguments are the same as those for the acoustic case presented by Zhang and Weglein (2005). For one interface model, because we choose the upper layer as the reference medium, there is no imaging task. The only task is inversion. In this case, all of the integration terms on the right side of equation 45 are zero and only the first five terms can be nonzero. Thus, we conclude that the integration terms (which care about duration) are imaging terms, and the first five terms are inversion terms.

The inversion and imaging terms (especially the imaging terms) become much more complicated after extending the acoustic case (Zhang and Weglein, 2005) to the elastic case. The integrand of the first three integral terms is the first-order approximation of the relative change in P-wave velocity. The derivatives $a_\gamma^{(1)'}$, $a_\rho^{(1)'}$, and $a_\mu^{(1)'}$ in front of those integrals are acting to correct the wrong locations caused by the inaccurate reference P-wave velocity. The other four terms with integrals are zero as $\beta_0\to 0$ because in this case $C\to\infty$.

We now test this approach numerically. For a single-interface 1D elastic medium case as shown in Figure 1, similar to the acoustic case, we use the analytic data (Clayton and Stolt, 1981; Weglein et al., 1986)

$$
\tilde{D}^{PP}(\nu_g,\theta)=R^{PP}(\theta)\frac{e^{2i\nu_g a}}{4\pi i\nu_g}
\tag{46}
$$

for the numerical tests. In this expression, a is the depth of the interface and the specific form of the reflection coefficient R^{PP} is as given by Foster et al. (1997). Substituting equation 46 into equation 39, Fourier transforming equation 39 over $2\nu_g$, and fixing $z>a$ and θ, we have

$$(1-\tan^2\theta)a_\rho^{(1)}(z)+(1+\tan^2\theta)a_\gamma^{(1)}(z)-8\frac{\beta_0^2}{\alpha_0^2}\sin^2\theta \times a_\mu^{(1)}(z)=4R^{PP}(\theta)H(z-a), \quad (47)$$

where H is the Heaviside step function. In this section, we numerically test the direct inversion approach on four models:

- Model 1 — shale (20% porosity) over oil sand (10% porosity): $\rho_0=2.32$ g/cm^3, $\rho_1=2.46$ g/cm^3; $\alpha_0=2627$ m/s, $\alpha_1=4423$ m/s; $\beta_0=1245$ m/s, $\beta_1=2939$ m/s.
- Model 2 — shale (20% porosity) over oil sand (20% porosity): $\rho_0=2.32$ g/cm^3, $\rho_1=2.27$ g/cm^3; $\alpha_0=2627$ m/s, $\alpha_1=3251$ m/s; $\beta_0=1245$ m/s, $\beta_1=2138$ m/s.
- Model 3 — shale (20% porosity) over oil sand (30% porosity): $\rho_0=2.32$ g/cm^3, $\rho_1=2.08$ g/cm^3; $\alpha_0=2627$ m/s, $\alpha_1=2330$ m/s; $\beta_0=1245$ m/s, $\beta_1=1488$ m/s.
- Model 4 — oil sand over wet sand, 20% porosity throughout: $\rho_0=2.27$ g/cm^3, $\rho_1=2.32$ g/cm^3; $\alpha_0=3251$ m/s, $\alpha_1=3507$ m/s; $\beta_0=2138$ m/s, $\beta_1=2116$ m/s.

To test and compare methods, we modeled the top of sand reflection for oil sands with porosities of 10%, 20%, and 30%. Models 1–3 used the same shale overburden, and they were designed so that model 1 had a class I AVO response, model 2 had a class II AVO response, and model 3 had a class III AVO response. An oil-water contact model was also constructed for the 20% porosity sand (model 4).

Among these four models, model 3, the high-porosity (30%) model, is typical of a weakly consolidated, shallow reservoir sand. Pore fluids have a large impact on the seismic response. Density, P-wave velocity, and the α/β ratio of the oil sand are lower than the density, P-wave velocity, and α/β ratio of the overlying shale. Consequently, there is a significant decrease in density and P-wave bulk modulus and an increase in shear modulus at the shale-oil-sand interface.

Model 2, the moderate-porosity (20%) model, represents deeper, more compacted reservoirs than model 3. Pore fluids have a large impact on seismic response, but the fluid effect is less than that of the high-porosity case. The overlying shale has high density compared to the reservoir sand, but the P-wave velocity of the oil sand exceeds that of the shale. Consequently, impedance contrast is reduced and S-wave information becomes more important for detecting the reservoir.

Model 1, the low-porosity (10%) model, represents a deep, well-consolidated reservoir sand. Pore fluids have little effect on the seismic response of the reservoir sand. It is difficult to distinguish oil sands from brine sands on the basis of seismic response. Impedance of the sand is higher than impedance of the shale.

Model 4 represents an oil-water contact in a sand of 20% porosity. At a fluid contact, density and P-wave velocity increase across the boundary between the oil zone and the wet zone. Because pore fluids have no affect on shear modulus, there is no change in shear modulus.

Using these four models, we can calculate the corresponding R^{PP} as a function of the incident angle. Then, choosing three angles, θ_1, θ_2, and θ_3, we can get the linear solutions for $a_\rho^{(1)}$, $a_\gamma^{(1)}$, and $a_\mu^{(1)}$ from equation 47 and the solutions for $a_\rho^{(2)}$, $a_\gamma^{(2)}$, and $a_\mu^{(2)}$ from equation 45.

The results of these calculations are shown in Figures 2–13. The left plot in each figure shows the results for the first order, and the

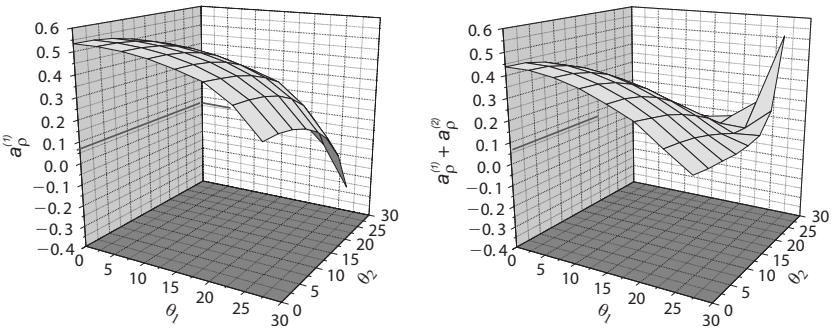

Figure 2. Model 1: shale (20% porosity) over oil sand (10% porosity), with parameters noted in the text. The exact value of a_ρ is 0.06 (bold black line). The linear approximation $a_\rho^{(1)}$ (left) and the sum of linear and first nonlinear approximations $a_\rho^{(1)}+a_\rho^{(2)}$ (right) correspond to different sets of angles θ_1 and θ_2 (degrees).

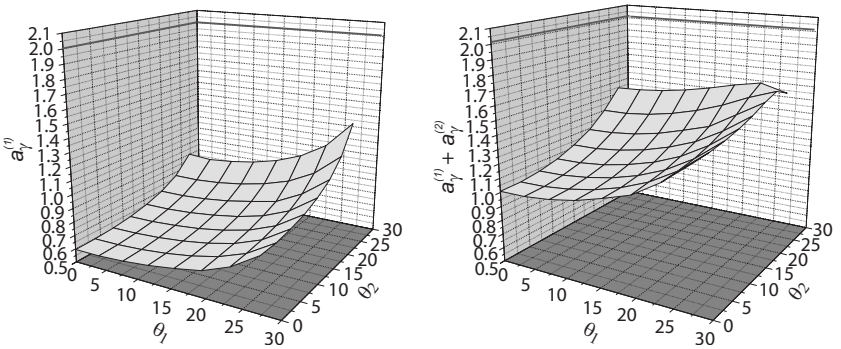

Figure 3. Model 1, same as Figure 2. The exact value of a_γ is 2.01 (bold black line). The linear approximation $a_\gamma^{(1)}$ (left) and the sum of linear and first nonlinear approximations $a_\gamma^{(1)}+a_\gamma^{(2)}$ (right) correspond to different sets of angles θ_1 and θ_2 (degrees).

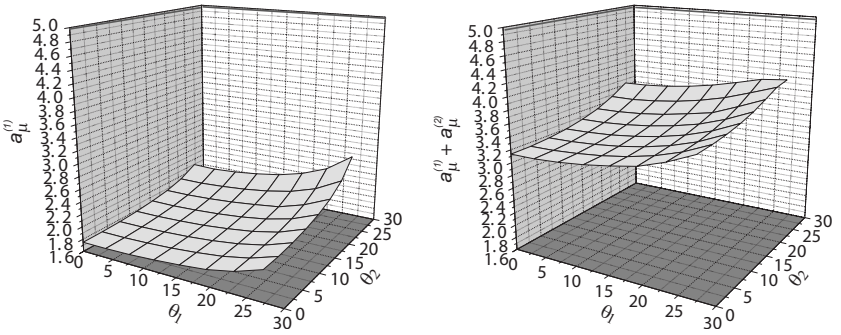

Figure 4. Model 1, same as Figure 2. The exact value of a_μ is 4.91 (bold black line). The linear approximation $a_\mu^{(1)}$ (left) and the sum of linear and first nonlinear approximations $a_\mu^{(1)}+a_\mu^{(2)}$ (right) correspond to different sets of angles θ_1 and θ_2 (degrees).

Figure 5. Model 2: shale (20% porosity) over oil sand (20% porosity), with parameters noted in the text. The exact value of a_ρ is -0.022 (bold black line). The linear approximation $a_\rho^{(1)}$ (left) and the sum of linear and first nonlinear approximations $a_\rho^{(1)} + a_\rho^{(2)}$ (right) correspond to different sets of angles θ_1 and θ_2 (degrees).

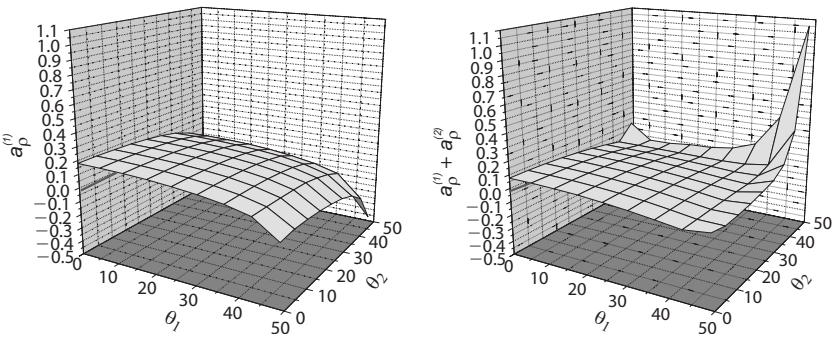

Figure 6. Model 2, same as Figure 5. The exact value of a_γ is 0.498 (bold black line). The linear approximation $a_\gamma^{(1)}$ (left) and the sum of linear and first nonlinear approximations $a_\gamma^{(1)} + a_\gamma^{(2)}$ (right) correspond to different sets of angles θ_1 and θ_2 (degrees).

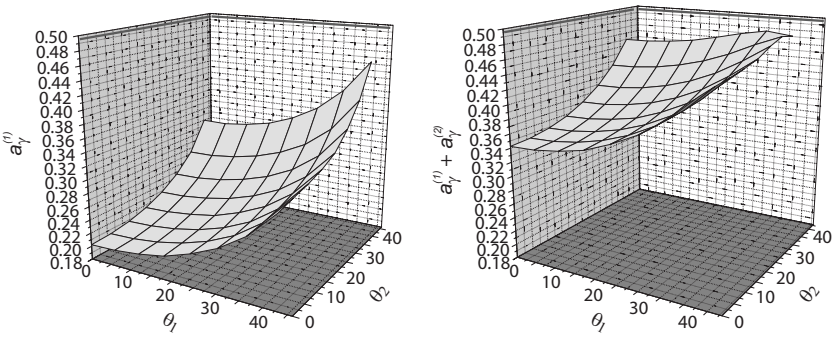

Figure 7. Model 2, same as Figure 5. The exact value of a_μ is 1.89 (bold black line). The linear approximation $a_\mu^{(1)}$ (left) and the sum of linear and first nonlinear approximations $a_\mu^{(1)} + a_\mu^{(2)}$ (right) correspond to different sets of angles θ_1 and θ_2 (degrees).

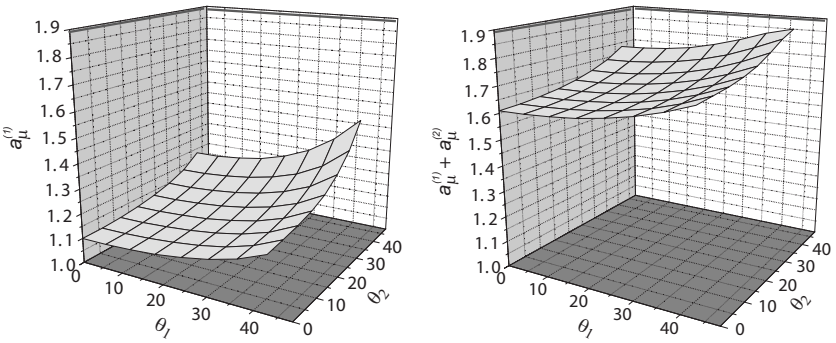

Figure 8. Model 3: shale (20% porosity) over oil sand (30% porosity), with parameters noted in the text. The exact value of a_ρ is -0.103 (bold black line). The linear approximation $a_\rho^{(1)}$ (left) and the sum of linear and first nonlinear approximations $a_\rho^{(1)} + a_\rho^{(2)}$ (right) correspond to different sets of angles θ_1 and θ_2 (degrees).

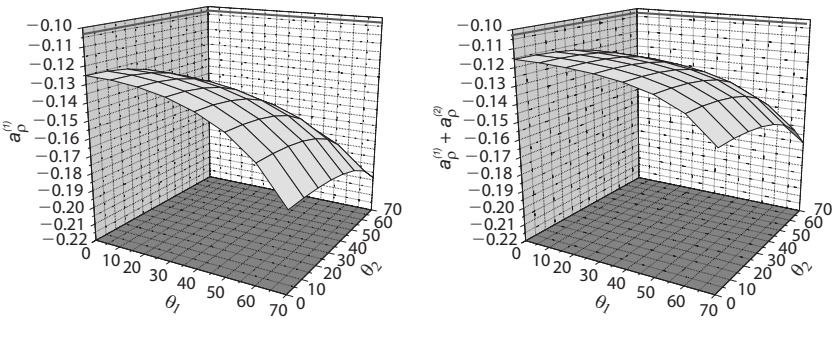

Figure 9. Model 3, same as Figure 8. The exact value of a_γ is -0.295 (bold black line). The linear approximation $a_\gamma^{(1)}$ (left) and the sum of linear and first nonlinear approximations $a_\gamma^{(1)} + a_\gamma^{(2)}$ (right) correspond to different sets of angles θ_1 and θ_2 (degrees).

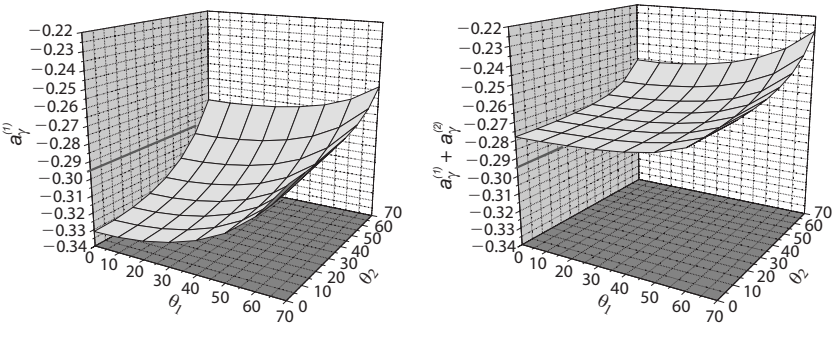

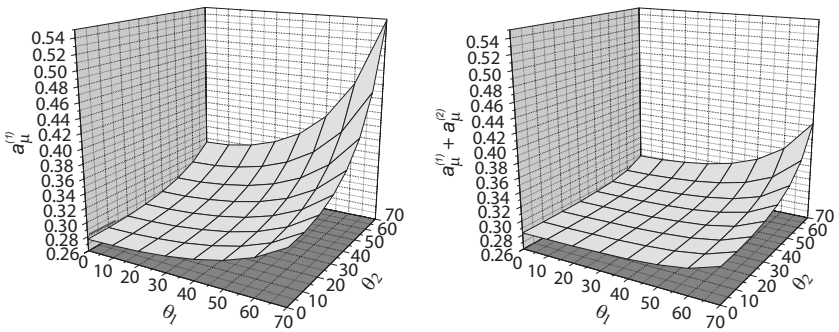

Figure 10. Model 3, same as Figure 8. The exact value of a_μ is 0.281 (bold black line). The linear approximation $a_\mu^{(1)}$ (left) and the sum of linear and first nonlinear approximations $a_\mu^{(1)} + a_\mu^{(2)}$ (right) correspond to different sets of angles θ_1 and θ_2 (degrees).

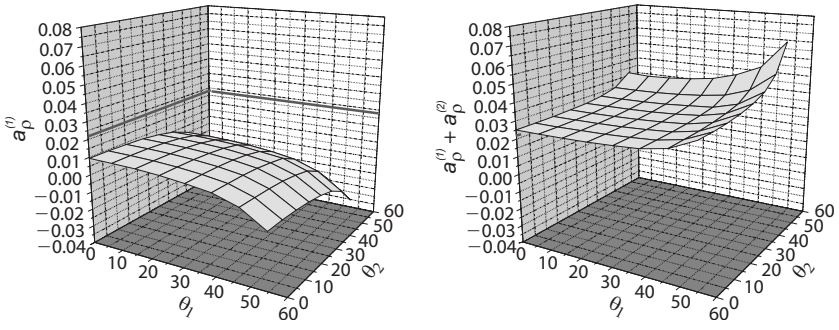

Figure 11. Model 4: oil sand over wet sand, 20% porosity throughout, with parameters noted in the text. The exact value of a_ρ is 0.022 (bold black line). The linear approximation $a_\rho^{(1)}$ (left) and the sum of linear and first nonlinear approximations $a_\rho^{(1)} + a_\rho^{(2)}$ (right) correspond to different sets of angles θ_1 and θ_2 (degrees).

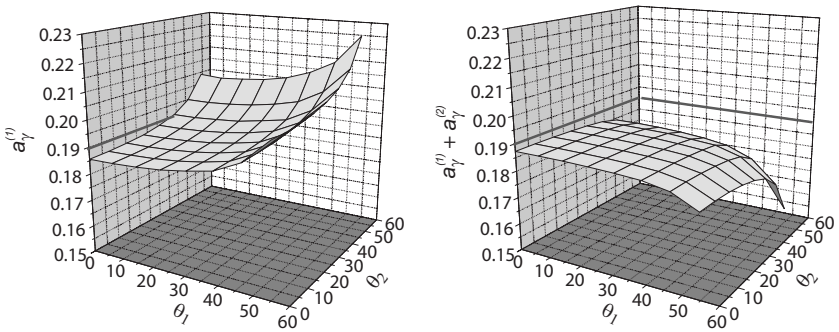

Figure 12. Model 4, same as Figure 11. The exact value of a_γ is 0.19 (bold black line). The linear approximation $a_\gamma^{(1)}$ (left) and the sum of linear and first nonlinear approximations $a_\gamma^{(1)} + a_\gamma^{(2)}$ (right) correspond to different sets of angles θ_1 and θ_2 (degrees).

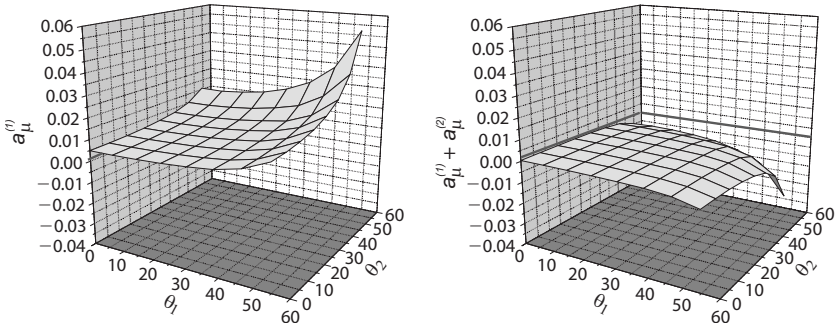

Figure 13. Model 4, same as Figure 11. The exact value of a_μ is 0.001 (bold black line). The linear approximation $a_\mu^{(1)}$ (left) and the sum of linear and first nonlinear approximations $a_\mu^{(1)} + a_\mu^{(2)}$ (right) correspond to different sets of angles θ_1 and θ_2 (degrees).

right plot shows the results for the first order plus the second order. In Figures 2–13, we illustrate the results for different sets of angles θ_1 and θ_2. The third angle θ_3 is fixed at zero.

The numerical results indicate that the second-order solutions provide improvements over the linear solutions for all four models. When the second term is added, the results approach much more closely the corresponding exact values, and the surfaces become flatter over a larger range of angles. But the degrees of improvement are different for each model. How accurately $\hat{D}^{PP}$ synthesizes $\hat{D}^{PS}$ and $\hat{D}^{SP}$ determines the degree of benefit provided by the nonlinear elastic approach. To synthesize the other components of the data from the $\hat{D}^{PP}$ component (e.g., $\hat{D}^{SP}$), for one interface example we first wrote equation 37 to the similar form of equation 47 in terms of

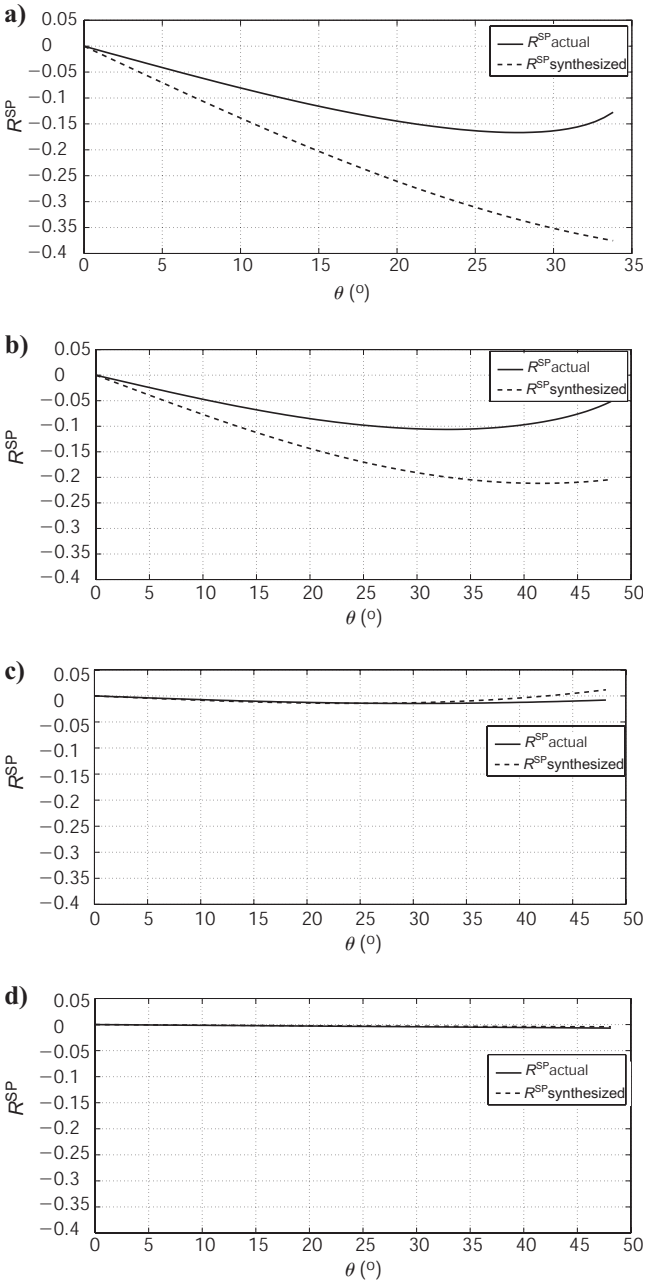

Figure 14. Comparison between synthesized values and actual values of R^{SP} for (a) model 1, (b) model 2, (c) model 3, and (d) model 4.

R^{SP} (the reflection coefficient shown in Figure 1). We then substituted the linear solutions from equation 47 in the equation for R^{SP} to derive R^{SP}. How accurately R^{SP} was synthesized for the four models is shown in Figure 14. All of the synthesized values in the figure were predicted using the linear results from equation 47. The actual values were calculated from the Zoeppritz equations.

In principle, the 2D elastic nonlinear direct inversion requires all components of data. However, in this section, we introduced an approach that requires only $\hat{D}^{PP}$ and approximately synthesizes the other required components. Based on this approach, we derived the direct nonlinear elastic inversion solution. Value is added to the results by the addition of the nonlinear inversion terms. Although $\hat{D}^{PP}$ alone can provide useful nonlinear direct inversion results, further value should be derived from field measurements of all components of the data that the method requires.

Using all components of data — Full direct nonlinear elastic inversion

Using all components of data, one consistent method to solve for the second-order terms is to first use the linear solutions of equations 35–38. We get the linear solution for $a_\rho^{(1)}$, $a_\gamma^{(1)}$, and $a_\mu^{(1)}$ in terms of $\hat{D}^{PP}$, $\hat{D}^{PS}$, $\hat{D}^{SP}$, and $\hat{D}^{SS}$ as follows:

$$\begin{pmatrix} a_\rho^{(1)} \\ a_\gamma^{(1)} \\ a_\mu^{(1)} \end{pmatrix} = (\mathbf{O}^T\mathbf{O})^{-1}\mathbf{O}^T \begin{pmatrix} \hat{D}^{PP} \\ \hat{D}^{PS} \\ \hat{D}^{SP} \\ \hat{D}^{SS} \end{pmatrix}, \tag{48}$$

where the matrix $\mathbf{O}$ is

$$\begin{pmatrix} -\frac{1}{4}\left(1-\frac{k_g^{PP2}}{\nu_g^{PP2}}\right) & -\frac{1}{4}\left(1+\frac{k_g^{PP2}}{\nu_g^{PP2}}\right) & \frac{2\beta_0^2 k_g^{PP2}}{\alpha_0^2(\nu_g^{PP2}+k_g^{PP2})} \\ -\frac{1}{4}\left(\frac{k_g^{PS}}{\nu_g^{PS}}+\frac{k_g^{PS}}{\eta_g^{PS}}\right) & 0 & -\frac{\beta_0^2}{2\omega^2}k_g^{PS}(\nu_g^{PS}+\eta_g^{PS})\left(1-\frac{k_g^{PS2}}{\nu_g^{PS}\eta_g^{PS}}\right) \\ \frac{1}{4}\left(\frac{k_g^{SP}}{\nu_g^{SP}}+\frac{k_g^{SP}}{\eta_g^{SP}}\right) & 0 & \frac{\beta_0^2}{2\omega^2}k_g^{SP}(\nu_g^{SP}+\eta_g^{SP})\left(1-\frac{k_g^{SP2}}{\nu_g^{SP}\eta_g^{SP}}\right) \\ -\frac{1}{4}\left(1-\frac{k_g^{SS2}}{\eta_g^{SS2}}\right) & 0 & -\left[\frac{k_g^{SS2}+\eta_g^{SS2}}{4\eta_g^{SS2}}-\frac{2k_g^{SS2}}{k_g^{SS2}+\eta_g^{SS2}}\right] \end{pmatrix}. \tag{49}$$

The superscripts PP, PS, SP, and SS on the wavenumbers are consistent with those on the data $\hat{D}$, and $\mathbf{O}^T$ is the transpose of $\mathbf{O}$. The superscript -1 denotes the inverse of the matrix $\mathbf{O}^T\mathbf{O}$.

If the arguments of $a_\rho^{(1)}$ and $a_\mu^{(1)}$ in equations 35–38 are equal, we need

$$-2\nu_g^{PP} = -\nu_g^{PS} - \eta_g^{PS} = -\nu_g^{SP} - \eta_g^{SP} = -2\eta_g^{SS}, \tag{50}$$

which leads to (Figure 15)

$$\begin{aligned} 2\frac{\omega}{\alpha_0}\cos\theta^{PP} &= \frac{\omega}{\alpha_0}\sqrt{1-\frac{\alpha_0^2}{\beta_0^2}\sin^2\theta^{PS}} + \frac{\omega}{\beta_0}\cos\theta^{PS} \\ &= \frac{\omega}{\alpha_0}\cos\theta^{SP} + \frac{\omega}{\beta_0}\sqrt{1-\frac{\beta_0^2}{\alpha_0^2}\sin^2\theta^{SP}} \\ &= 2\frac{\omega}{\beta_0}\cos\theta^{SS}. \end{aligned} \tag{51}$$

From expression 51, given θ^{PP}, we can find the corresponding angles θ^{PS}, θ^{SP}, and θ^{SS}, which appear in $\mathbf{O}$:

$$\theta^{PS} = \cos^{-1}\left[\frac{4b^2\cos^2\theta^{PP} + 1 - b^2}{4b\cos\theta^{PP}}\right], \tag{52}$$

$$\theta^{SP} = \cos^{-1}\left[\frac{4b^2\cos^2\theta^{PP} - 1 + b^2}{4b^2\cos\theta^{PP}}\right], \tag{53}$$

$$\theta^{SS} = \cos^{-1}(b\cos\theta^{PP}), \tag{54}$$

where $b = \beta_0/\alpha_0$. Then, we can similarly get the solution for $a_\rho^{(2)}$, $a_\gamma^{(2)}$, and $a_\mu^{(2)}$ in terms of $a_\rho^{(1)}$, $a_\gamma^{(1)}$, and $a_\mu^{(1)}$:

$$\begin{pmatrix} a_\rho^{(2)} \\ a_\gamma^{(2)} \\ a_\mu^{(2)} \end{pmatrix} = (\mathbf{O}^T\mathbf{O})^{-1}\mathbf{O}^T\mathbf{Q}, \tag{55}$$

where $\mathbf{Q}$ is in terms of $a_\rho^{(1)}$, $a_\gamma^{(1)}$, and $a_\mu^{(1)}$. Based on this idea, the form of the nonlinear solution for equation 41 is the same as equation 45. In the $(k_s,z_s;k_g,z_g;\omega)$ domain, we get the other three solutions for equations 42–44. The solution for equation 42 is

$$\begin{aligned}
-\frac{1}{4}\left(\frac{k_g}{\nu_g}+\frac{k_g}{\eta_g}\right)a_\rho^{(2)}(z) - \frac{\beta_0^2}{2\omega^2}k_g(\nu_g+\eta_g)\left(1-\frac{k_g^2}{\nu_g\eta_g}\right)&\\
a_\mu^{(2)}(z) = -\left[\left(\frac{1}{2}+\frac{1}{C+1}\right)\frac{1}{\eta_g\nu_g^2}\left(\frac{\beta_0^4}{\alpha_0^4}Ck_g^3\right.\right.&\\
-3\frac{\beta_0^2}{\alpha_0^2}Ck_g^5\frac{\beta_0^2}{\omega^2} - k_g^3\nu_g^2\frac{\beta_0^2}{\omega^2} + 2k_g^5\nu_g^2\frac{\beta_0^4}{\omega^4} + 2Ck_g^7\frac{\beta_0^4}{\omega^4}\Big)&\\
+\left(\frac{1}{2}-\frac{1}{C+1}\right)\frac{1}{\eta_g\nu_g^2}\left(\frac{\beta_0^2}{\alpha_0^2}Ck_g^3\nu_g^2\frac{\beta_0^2}{\omega^2} + 2\frac{\beta_0^2}{\alpha_0^2}k_g^5\frac{\beta_0^2}{\omega^2}\right.&\\
-2Ck_g^5\nu_g^2\frac{\beta_0^4}{\omega^4} - \frac{\beta_0^2}{\alpha_0^2}k_g^3 + k_g^5\frac{\beta_0^2}{\omega^2} - 2k_g^7\frac{\beta_0^4}{\omega^4}\Big) + \left(\frac{1}{2C}\right.&\\
+\frac{1}{C+1}\Big)\frac{1}{4\eta_g^2\nu_g}\left(6k_g^3 - 12k_g^5\frac{\beta_0^2}{\omega^2} - k_g\frac{\omega^2}{\beta_0^2} + 8k_g^7\frac{\beta_0^4}{\omega^4}\right.&\\
+8C^3\nu_g^2k_g^5\frac{\beta_0^4}{\omega^4} - 4\frac{\beta_0^2}{\alpha_0^2}C^3\nu_g^2k_g^3\frac{\beta_0^2}{\omega^2}\Big) - \left(\frac{1}{2C}\right.&\\
-\frac{1}{C+1}\Big)\frac{1}{4\eta_g\nu_g^2}\left(4\frac{\beta_0^2}{\alpha_0^2}k_g^3 - 8k_g^5\frac{\beta_0^2}{\omega^2} - k_g\frac{\omega^2}{\alpha_0^2} + 2k_g^3\right.&\\
-4C\nu_g^2k_g^3\frac{\beta_0^2}{\omega^2} + 8C\nu_g^2k_g^5\frac{\beta_0^4}{\omega^4} - 4\frac{\beta_0^2}{\alpha_0^2}k_g^5\frac{\beta_0^2}{\omega^2} + 8k_g^7\frac{\beta_0^4}{\omega^4}\Big)&\\
-\frac{\beta_0^2}{\alpha_0^2}\frac{k_g^3}{\nu_g}\frac{\beta_0^2}{\omega^2} + \frac{k_g}{2\eta_g}\left(2k_g^2\frac{\beta_0^2}{\omega^2}-1\right)\Big][a_\mu^{(1)}(z)]^2 - \Big[\Big(\frac{1}{2}&\\
+\frac{1}{C+1}\Big)\frac{k_g}{8\eta_g\nu_g^2}(Ck_g^2+\nu_g^2) - \left(\frac{1}{2}\right.&\\
-\frac{1}{C+1}\Big)\frac{k_g}{8\eta_g\nu_g^2}(k_g^2+C\nu_g^2) + \left(\frac{1}{2C}\right.&\\
+\frac{1}{C+1}\Big)\frac{k_g}{8\eta_g^2\nu_g}(C^3\nu_g^2+k_g^2) - \left(\frac{1}{2C}\right.&\\
-\frac{1}{C+1}\Big)\frac{k_g}{8\eta_g\nu_g^2}(k_g^2+C\nu_g^2)\Big][a_\rho^{(1)}(z)]^2 - \Big[\Big(\frac{1}{2}&\\
+\frac{1}{C+1}\Big)\frac{\beta_0^2}{\alpha_0^2}\frac{1}{4\nu_g^3}k_g(k_g^2-\nu_g^2) + \left(\frac{1}{2}\right.&\\
-\frac{1}{C+1}\Big)\frac{1}{4\eta_g\nu_g^2}\left(k_g\frac{\omega^2}{\alpha_0^2} - 2\frac{\beta_0^2}{\alpha_0^2}k_g^3\right) + \frac{\beta_0^2}{\alpha_0^2}\frac{k_g}{2\nu_g}\Big]&\\
\times a_\mu^{(1)}(z)a_\gamma^{(1)}(z) + \Big[\Big(\frac{1}{2}+\frac{1}{C+1}\Big)\frac{k_g(k_g^2+\nu_g^2)}{8\nu_g^3} - \left(\frac{1}{2}\right.&\\
-\frac{1}{C+1}\Big)\frac{k_g(k_g^2+\nu_g^2)}{8\eta_g\nu_g^2}\Big]a_\rho^{(1)}(z)a_\gamma^{(1)}(z) - \Big[\Big(\frac{1}{2}&\\
+\frac{1}{C+1}\Big)\frac{1}{4\eta_g\nu_g^2}\left(3\frac{\beta_0^2}{\alpha_0^2}Ck_g^3 + \nu_g^2k_g - 4Ck_g^5\frac{\beta_0^2}{\omega^2}\right.&\\
-4k_g^3\nu_g^2\frac{\beta_0^2}{\omega^2}\Big) - \left(\frac{1}{2}-\frac{1}{C+1}\right)\frac{1}{4\eta_g\nu_g^2}\left(\frac{\beta_0^2}{\alpha_0^2}C\nu_g^2k_g + k_g^3\right.&\\
-4k_g^5\frac{\beta_0^2}{\omega^2} - 4Ck_g^3\nu_g^2\frac{\beta_0^2}{\omega^2} + 2\frac{\beta_0^2}{\alpha_0^2}k_g^3\Big) + \left(\frac{1}{2C}\right.&\\
+\frac{1}{C+1}\Big)\frac{1}{4\eta_g^2\nu_g}\left(k_g^3 - 2k_g^5\frac{\beta_0^2}{\omega^2} + \frac{\beta_0^2}{\alpha_0^2}C^3\nu_g^2k_g\right.&\\
-4C^3\nu_g^2k_g^3\frac{\beta_0^2}{\omega^2} - \frac{1}{2}k_g\frac{\omega^2}{\beta_0^2} + 2C^2\nu_g^2k_g^3\frac{\beta_0^2}{\omega^2}\Big) - \left(\frac{1}{2C}\right.&\\
-\frac{1}{C+1}\Big)\frac{1}{4\eta_g\nu_g^2}\left(C\nu_g^2k_g - 2C\nu_g^2k_g^3\frac{\beta_0^2}{\omega^2} + \frac{\beta_0^2}{\alpha_0^2}k_g^3\right.&\\
-2k_g^5\frac{\beta_0^2}{\omega^2} + 2C^2\nu_g^2k_g^3\frac{\beta_0^2}{\omega^2} - 2C\nu_g^2k_g^3\frac{\beta_0^2}{\omega^2} - \frac{1}{2}k_g\frac{\omega^2}{\beta_0^2}\Big)\Big]&\\
\times a_\rho^{(1)}(z)a_\mu^{(1)}(z) + \text{other terms with integrals,}
\end{aligned} \tag{56}$$

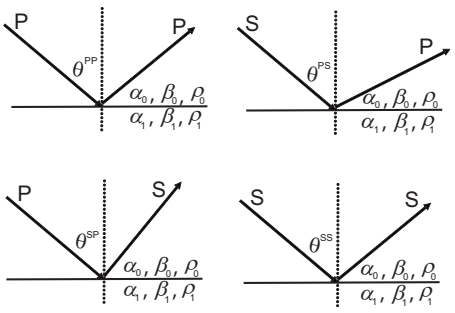

Figure 15. Different incident angles for different wave types.

where details about the other terms with integrals are provided by Zhang (2006). Similarly, for the right side of the following two equations, we also show only the inversion terms; the terms with integrals are not given in detail.

The solution for equation 43 is

$$\begin{aligned}
&\frac{1}{4}\left(\frac{k_g}{\nu_g}+\frac{k_g}{\eta_g}\right)a_\rho^{(2)}(z)+\frac{\beta_0^2}{2\omega^2}k_g(\nu_g+\eta_g)\left(1-\frac{k_g^2}{\nu_g\eta_g}\right)a_\mu^{(2)}(z)\\
&=\left\{-\frac{1}{2\eta_g\nu_g^2}\left[2(C-1)\nu_g^2k_g^5\frac{\beta_0^4}{\omega^4}+\left(1\right.\right.\right.\\
&\quad\left.-\frac{\beta_0^2}{\alpha_0^2}C\right)\nu_g^2k_g^3\frac{\beta_0^2}{\omega^2}\Big]-\frac{\beta_0^2}{\alpha_0^2}\frac{k_g^3}{\nu_g}\frac{\beta_0^2}{\omega^2}+\frac{k_g}{2\eta_g}\left(2k_g^2\frac{\beta_0^2}{\omega^2}-1\right)\\
&\quad+\left(\frac{1}{2C}+\frac{1}{C+1}\right)\frac{1}{4\eta_g^2\nu_g}\left(6k_g^3-12k_g^5\frac{\beta_0^2}{\omega^2}-k_g\frac{\omega^2}{\beta_0^2}\right.\\
&\quad+8k_g^7\frac{\beta_0^4}{\omega^4}+8C^3\nu_g^2k_g^5\frac{\beta_0^4}{\omega^4}-4\frac{\beta_0^2}{\alpha_0^2}C^3\nu_g^2k_g^3\frac{\beta_0^2}{\omega^2}\Big)-\left(\frac{1}{2C}\right.\\
&\quad-\frac{1}{C+1}\Big)\frac{1}{4\eta_g\nu_g^2}\left(4\frac{\beta_0^2}{\alpha_0^2}k_g^3-8k_g^5\frac{\beta_0^2}{\omega^2}-k_g\frac{\omega^2}{\alpha_0^2}+2k_g^3\right.\\
&\quad\left.\left.-4C\nu_g^2k_g^3\frac{\beta_0^2}{\omega^2}+8C\nu_g^2k_g^5\frac{\beta_0^4}{\omega^4}-4\frac{\beta_0^2}{\alpha_0^2}k_g^5\frac{\beta_0^2}{\omega^2}+8k_g^7\frac{\beta_0^4}{\omega^4}\right)\right\}\\
&\quad\times[a_\mu^{(1)}(z)]^2+\left[\left(\frac{1}{2}+\frac{1}{C+1}\right)\frac{k_g}{8\eta_g\nu_g^2}(Ck_g^2+\nu_g^2)\right.\\
&\quad-\left(\frac{1}{2}-\frac{1}{C+1}\right)\frac{k_g}{8\eta_g\nu_g^2}(k_g^2+C\nu_g^2)+\left(\frac{1}{2C}\right.\\
&\quad+\frac{1}{C+1}\Big)\frac{k_g}{8\eta_g^2\nu_g}(C^3\nu_g^2+k_g^2)-\left(\frac{1}{2C}\right.\\
&\quad\left.-\frac{1}{C+1}\Big)\frac{k_g}{8\eta_g\nu_g^2}(k_g^2+C\nu_g^2)\right]\\
&\quad\times[a_\rho^{(1)}(z)]^2+\left[\left(\frac{1}{2}+\frac{1}{C+1}\right)\frac{\beta_0^2}{\alpha_0^2}\frac{1}{4\nu_g^3}k_g(k_g^2-\nu_g^2)\right.\\
&\quad+\left(\frac{1}{2}-\frac{1}{C+1}\right)\frac{1}{4\eta_g\nu_g^2}\left(k_g\frac{\omega^2}{\alpha_0^2}-2\frac{\beta_0^2}{\alpha_0^2}k_g^3\right)\\
&\quad\left.+\frac{\beta_0^2}{\alpha_0^2}\frac{k_g}{2\nu_g}\right]a_\mu^{(1)}(z)a_\gamma^{(1)}(z)-\left[\left(\frac{1}{2}\right.\right.\\
&\quad+\frac{1}{C+1}\Big)\frac{k_g(k_g^2+\nu_g^2)}{8\nu_g^3}-\left(\frac{1}{2}\right.\\
&\quad\left.-\frac{1}{C+1}\Big)\frac{k_g(k_g^2+\nu_g^2)}{8\eta_g\nu_g^2}\right]a_\rho^{(1)}(z)a_\gamma^{(1)}(z)-\left[\left(\frac{1}{2}\right.\right.\\
&\quad+\frac{1}{C+1}\Big)\frac{1}{4\eta_g\nu_g^2}\left(2\nu_g^2k_g^3\frac{\beta_0^2}{\omega^2}-\nu_g^2k_g+2Ck_g^5\frac{\beta_0^2}{\omega^2}\right.\\
&\quad-\frac{\beta_0^2}{\alpha_0^2}Ck_g^3\Big)-\left(\frac{1}{2}-\frac{1}{C+1}\right)\frac{1}{4\eta_g\nu_g^2}\left(2C\nu_g^2k_g^3\frac{\beta_0^2}{\omega^2}\right.\\
&\quad-\frac{\beta_0^2}{\alpha_0^2}C\nu_g^2k_g+2k_g^5\frac{\beta_0^2}{\omega^2}-k_g^3\Big)-\left(\frac{1}{2C}\right.\\
&\quad+\frac{1}{C+1}\Big)\frac{1}{4\eta_g^2\nu_g}\left(3k_g^3+\frac{\beta_0^2}{\alpha_0^2}C^3\nu_g^2k_g-4C^3\nu_g^2k_g^3\frac{\beta_0^2}{\omega^2}\right.\\
&\quad-4k_g^5\frac{\beta_0^2}{\omega^2}-\frac{1}{2}k_g\frac{\omega^2}{\beta_0^2}\Big)+\left(\frac{1}{2C}-\frac{1}{C+1}\right)\frac{1}{4\eta_g\nu_g^2}\left(C\nu_g^2k_g\right.\\
&\quad+2k_g^3+\frac{\beta_0^2}{\alpha_0^2}k_g^3-4k_g^5\frac{\beta_0^2}{\omega^2}-4Ck_g^3\nu_g^2\frac{\beta_0^2}{\omega^2}-\frac{1}{2}k_g\frac{\omega^2}{\beta_0^2}\Big)\\
&\quad\left.-(C-1)\frac{k_g^3}{2\eta_g}\frac{\beta_0^2}{\omega^2}\right]a_\rho^{(1)}(z)a_\mu^{(1)}(z)\\
&\quad+\text{other terms with integrals.}
\end{aligned}\tag{57}$$

The solution for equation 44 is

$$\begin{aligned}
&-\frac{1}{4}\left(1-\frac{k_g^2}{\eta_g^2}\right)a_\rho^{(2)}(z)-\left[\frac{k_g^2+\eta_g^2}{4\eta_g^2}-\frac{2k_g^2}{k_g^2+\eta_g^2}\right]a_\mu^{(2)}(z)=\\
&\quad-\left\{\frac{1}{8\eta_g^4}\left(8k_g^2\eta_g^2-\frac{\omega^4}{\beta_0^4}\right)-\frac{1}{4\eta_g^2}\left(\frac{\omega^2}{\beta_0^2}-4\frac{\beta_0^2}{\omega^2}\eta_g^2k_g^2\right)\right.\\
&\quad-\frac{\beta_0^2}{\alpha_0^2}k_g^2\frac{\beta_0^2}{\omega^2}+\frac{1}{\eta_g^2(C+1)}\left[k_g^2\left(\frac{\beta_0^4}{\alpha_0^4}C^2-1\right)\right.\\
&\quad\left.\left.-4k_g^4\frac{\beta_0^2}{\omega^2}\left(\frac{\beta_0^2}{\alpha_0^2}C^2-1\right)+4k_g^6\frac{\beta_0^4}{\omega^4}(C^2-1)\right]\right\}[a_\mu^{(1)}(z)]^2\\
&\quad-\left[\frac{1}{8\eta_g^4}(\eta_g^4-k_g^4)+\frac{1}{4\eta_g^2}k_g^2(C-1)\right][a_\rho^{(1)}(z)]^2+\left\{\frac{k_g^2}{\eta_g^2}\right.\\
&\quad-\frac{1}{\eta_g^2(C+1)}\left[k_g^2\left(\frac{\beta_0^2}{\alpha_0^2}C^2-1\right)-2\frac{\beta_0^2}{\omega^2}k_g^4(C^2\right.\\
&\quad\left.\left.-1)\right]\right\}a_\mu^{(1)}(z)a_\rho^{(1)}(z)+\text{other terms with integrals.}
\end{aligned}\tag{58}$$

After we solve all four of the second-order equations, our future research will be to perform numerical tests with all components of data available. In principle, $\hat{D}^{\text{PS}}$ and $\hat{D}^{\text{SP}}$ differ only by a minus sign; therefore, they do not provide independent equations. However, given the practical difficulties associated with noise and with acquiring and processing converted wave data, it is almost certain that practical benefits will accrue from using data that would otherwise be redundant.

DISCUSSION

The standard AVO methods used today are all indirect, seeking an aligned objective cost function, or proxy, in place of a direct inverse solution. Although such methods are sometimes useful, there are

ambiguities and conceptual and practical pitfalls associated with violating the fundamental physics provided by direct nonlinear inversion. The use of indirect methods ought to indicate that direct methods are unavailable. When direct methods are available, they are the preferred choice in all fields of problem solving; they provide the clearest solutions and give us confidence in the algorithms we use and the input data required.

The inverse scattering series provides the ability to directly image and directly nonlinearly invert across a dipping and specular or diffractive boundary, all without subsurface information. Further tests and analysis of the concepts presented here are being pursued and will be the subject of future publications.

The 1D elastic formulation tested here is only a small part of the capability of the concepts presented. The assumptions and limitations of the specific algorithm tested in this paper are that (1) the earth has variation only in depth, (2) multiples have been removed, (3) the medium above the single horizontal reflector is known, and (4) reflection data with accurate reflection coefficients are available as input to the inversion. Although this is a strict list of assumptions, the tests nevertheless represent the first direct inversion of the forward Zoeppritz equations. Our algorithm requires further testing in a petroleum development environment, where surface seismic data are tied to well measurements and where the procedure can be conducted using reflection data away from the well.

Our direct AVO inversion method, in this series of initial tests, shares with other AVO applications many of the typical assumptions, such as knowledge of the overburden, lack of multiples, true-amplitude reflection data, and a horizontal reflector. Those assumptions and limitations will be relaxed and removed in future work.

CONCLUSIONS

We have developed a framework and an algorithm that can be used for identifying exploration targets more accurately. Elastic nonlinear direct inversion requires all components of seismic data. In this paper, we have analyzed an algorithm that inputs only PP data. Although PP data alone can provide useful nonlinear direct inversion results when we use the PP data to synthesize PS, SP, and SS components, further value should be derived from measuring all components of data in the field.

If all components are available, our method consistently solves for all second-order terms. Further tests using all components of the data (in a 2D world) are under way, which we will compare to our results with real PP data and synthesized PS, SP, and SS data components.

ACKNOWLEDGMENTS

The M-OSRP sponsors are thanked for supporting this research. We are grateful to Robert Keys and Douglas Foster for useful comments and suggestions. We have been partially funded by and are grateful for NSF-CMG award DMS-0327778 and DOE Basic Sciences award DE-FG02-05ER15697. H. Zhang would also like to thank ConocoPhillips for permission to publish this work.

REFERENCES

Aki, K., and P. G. Richards, 2002, Quantitative seismology, 2nd ed.: University Science Books.

Araújo, F. V., 1994, Linear and non-linear methods derived from scattering theory: Backscattered tomography and internal multiple attenuation: Ph.D. dissertation, Universidade Federal da Bahia, Brazil.

Carvalho, P. M., 1992, Free-surface multiple reflection elimination method based on nonlinear inversion of seismic data: Ph.D. dissertation, Universidade Federal da Bahia, Brazil.

Clayton, R. W., and R. H. Stolt, 1981, A Born-WKBJ inversion method for acoustic reflection data: Geophysics, **46**, 1559–1567.

Foster, D. J., R. G. Keys, and D. P. Schmitt, 1997, Detecting subsurface hydrocarbons with elastic wavefields: Institute for Mathematics and its Applications, **90**, 195.

Innanen, K. A., and A. B. Weglein, 2004, Linear inversion for absorptive/dispersive medium parameters: 74th Annual International Meeting, SEG, Expanded Abstracts, 1834–1837.

———, 2005, Towards nonlinear construction of a *Q*-compensation operator directly from measured seismic reflection data: 75th Annual International Meeting, SEG, Expanded Abstracts, 1693–1696.

Liu, F., B. G. Nita, A. B. Weglein, and K. A. Innanen, 2004, Inverse scattering series in the presence of lateral variations: University of Houston Mission-Oriented Seismic Research Program (M-OSRP) Annual Report 3, 182–204.

Liu, F., and A. B. Weglein, 2003, Initial analysis of the inverse scattering series for a variable background: University of Houston Mission-Oriented Seismic Research Program (M-OSRP) Annual Report 2, 210–225.

Liu, F., A. B. Weglein, K. A. Innanen, and B. G. Nita, 2005, Extension of the non-linear depth imaging capability of the inverse scattering series to multidimensional media: Strategies and numerical results: 9th Annual Congress, Brazilian Geophysical Society, Expanded Abstracts.

Matson, K. H., 1997, An inverse-scattering series method for attenuating elastic multiples from multicomponent land and ocean bottom seismic data: Ph.D. dissertation, University of British Columbia.

Ramírez, A. C., and A. B. Weglein, 2005, An inverse scattering internal multiple elimination method: Beyond attenuation, a new algorithm and initial tests: 75th Annual International Meeting, SEG, Expanded Abstracts, 2115–2118.

Shaw, S. A., and A. B. Weglein, 2003, Imaging seismic reflection data at the correct depth without specifying an accurate velocity model: Initial examples of an inverse scattering subseries, *in* C. H. Chen, ed., Frontiers of remote sensing information processing: World Scientific Publishing Company, 469–484.

———, 2004, A leading order imaging series for prestack data acquired over a laterally invariant acoustic medium. Part II: Analysis for data missing low frequencies: University of Houston Mission-Oriented Seismic Research Program (M-OSRP) Annual Report 3, 140–167.

Shaw, S. A., A. B. Weglein, D. J. Foster, K. H. Matson, and R. G. Keys, 2003a, Convergence properties of a leading order depth imaging series: 73rd Annual International Meeting, SEG, Expanded Abstracts, 937–940.

———, 2003b, Isolation of a leading order depth imaging series and analysis of its convergence properties: University of Houston Mission-Oriented Seismic Research Program (M-OSRP) Annual Report 2, 157–195.

———, 2004, Isolation of a leading order depth imaging series and analysis of its convergence properties: Journal of Seismic Exploration, **2**, 157–195.

Sheriff, R. E., and L. P. Geldart, 1994, Exploration seismology, 2nd ed.: Cambridge University Press.

Weglein, A. B., 2007, A note: Data requirements for inverse theory: University of Houston Mission-Oriented Seismic Research Program (M-OSRP) Annual Report 6, 80–95.

Weglein, A. B., F. V. Araújo, P. M. Carvalho, R. H. Stolt, K. H. Matson, R. T. Coates, D. Corrigan, D. J. Foster, S. A. Shaw, and H. Zhang, 2003, Inverse scattering series and seismic exploration: Inverse Problems, **19**, R27-R83.

Weglein, A. B., D. J. Foster, K. H. Matson, S. A. Shaw, P. M. Carvalho, and D. Corrigan, 2002, Predicting the correct spatial location of reflectors without knowing or determining the precise medium and wave velocity: Initial concept, algorithm and analytic and numerical example: Journal of Seismic Exploration, **10**, 367–382.

Weglein, A. B., F. A. Gasparotto, P. M. Carvalho, and R. H. Stolt, 1997, An inverse-scattering series method for attenuating multiples in seismic reflection data: Geophysics, **62**, 1975–1989.

Weglein, A. B., P. B. Violette, and T. H. Keho, 1986, Using multiparameter Born theory to obtain certain exact multiparameter inversion goals: Geophysics, **51**, 1069–1074.

Zhang, H., 2006, Direct non-linear acoustic and elastic inversion: Towards fundamentally new comprehensive and realistic target identification: Ph.D. dissertation, University of Houston.

Zhang, H., and A. B. Weglein, 2005, The inverse scattering series for tasks associated with primaries: Depth imaging and direct nonlinear inversion of 1D variable velocity and density acoustic media: 75th Annual International Meeting, SEG, Expanded Abstracts, 1705–1708.